Dynamics of Flow and Diffusion of Adsorbing Gases in Al_2O_3 and Pd-Al_2O_3 Pellets

Meltem Dogan and Gülsen Dogu
Dept. of Chemical Engineering, Gazi University, 06570 Maltepe, Ankara, Turkey

A nonisobaric pulse-response technique was proposed for the simultaneous analysis of flow and diffusion of adsorbing tracers in porous solids. Relative contributions of viscous flow, Knudsen flow, surface flow, and effective diffusion of adsorbing (hydrogen and carbon dioxide) and inert (helium) tracers in alumina and Pd-alumina pellets were evaluated. Hydrogen permeability was shown to increase by Pd impregnation into alumina, due to the contribution of surface flow, especially at low temperatures. The tortuosity factor, corresponding to the viscous and Knudsen flow, was found to be less than the tortuosity factors evaluated from effective diffusivities obtained from isobaric pulse-response experiments.

Introduction

Gas transport in porous solids depends on the nature of the diffusing gases, pore structure of the solid, temperature, and pressure. Combined diffusion and viscous flow, observed under nonisobaric conditions, is rather complex, involving Knudsen diffusion, molecular diffusion, surface diffusion, and viscous flow.

In the early literature, a number of models were derived to explain the gas transport mechanism in porous substrates. Diffusion and viscous flow in a fine capillary were analyzed in the early studies of Scott and Dullien (1962), Evans et al. (1962), Wakao et al. (1965), and Nicholson and Petropoulos (1975, 1978, 1981). Allawi and Gunn (1987) reported a nice review of the earlier studies, and compared the predictions of the dusty gas model with some experimental data obtained in a steady-state Wicke-Kallenbach-type diffusion cell, under nonisobaric conditions. Darcy's equation was generally used in describing the viscous flow term in porous solids. More recently, Beuscher and Gooding (1998) used a similar model to describe the transport of binary gas mixtures through porous membrane supports.

Knudsen diffusion, molecular diffusion, viscous flow, surface diffusion, and capillary condensation may contribute to the transport of gases through porous membranes. Contribution of the surface diffusion to the transport of adsorbing gases may become significant at low temperatures. The permeabilities of several gases (H_2, N_2, O_2, Ar, He, H_2S, CO_2, and C_3H_6) in a silicon-based membrane tube were investigated by Li and Hwang (1992) in the pressure range of 170–446 kPa and in the temperature range of 25–700°C. The gas permeability including Knudsen flow and surface flow, decreased with increasing temperature because of the decrease of the surface concentration of the adsorbate, while total permeability increased with an increase of pressure, because of increased surface concentration.

The permeability of a specific gas through a porous solid may be improved by surface modification (Okubo and Inoue, 1988; Miller and Koros, 1990). Impregnation with a metal salt is the most common method of modification (Champagnie et al., 1992). By such surface modification, permeability of a specific gas through the porous solid may be improved. Also, pore-size distribution of the solid may be altered by such a surface modification. Another application of such a modification is to improve the catalytic activity of the solid. Palladium is the most popular metal used in surface modification to improve the permeability and separation factor of hydrogen as compared to other gases (Chai et al., 1992; Konno et al., 1988).

In recent studies, Pd impregnated silica and/or alumina and Pd-alumina (or silica) composite membranes were recommended, especially to improve hydrogen separation (Okubo and Inoue, 1988; Lee et al., 1994; Uemiya et al., 1997; So et al., 1998; Itoh et al., 2000; Goto et al., 2000). It is well known that hydrogen dissolves in Pd to a remarkable degree and diffuses through the metal. This process was expected to

Correspondence concerning this article should be addressed to G. Dogu.

be increased by the increase in temperature and hydrogen pressure (Goto et al., 2000). Hydrogen absorption in Pd and its permeation was found to be appreciable, especially at temperatures over 200°C. The diffusion coefficient of hydrogen within the Pd metal was estimated to increase from 5.5×10^{-11} m^2/s to 9.2×10^{-10} m^2/s with an increase in temperature from 40°C to 200°C (Goto et al., 2000). On the other hand, one expects a significant surface diffusion of hydrogen on the Pd metal surface, especially at low temperatures. The decrease in the adsorbed concentration of hydrogen with an increase in temperature will cause a decrease in the contribution of surface diffusion at higher temperatures. More recently, in our previous study (Dogan and Dogu, 2003), significant enhancement of hydrogen diffusivity was reported at low temperatures due to the contribution of surface diffusion in Pd-impregnated alumina pellets.

The moment analysis in chromatography has been applied to measure the transport rate and adsorption parameters in porous solids. In earlier articles, this method was applied to beds of porous solids (Schneider and Smith, 1968; Cerro and Smith, 1970; Dougharty, 1972). More recently, the adsorption of sulfur dioxide on molecular sieve 13X and activated carbon was investigated in a packed column using the nonisobaric pulse chromatographic technique (Kopac, 1999). A similar technique was used to evaluate effective diffusion coefficients in a macroreticular resin catalyst (Oktar et al., 1999). In the single-pellet moment technique developed by Dogu and Smith (1975, 1976), the interpellet mass transfer and the axial dispersion effects were eliminated. This technique was used by a number of investigators for the evaluation of effective diffusivities, adsorption equilibrium, and rate constants and reaction rate constants in porous solids. Intraparticle forced convection effects might have a significant influence on catalyst diffusivity measurements (Rodrigues et al., 1982). Dogu et al. (1989) investigated viscous flow and diffusion of nonadsorbing gases in porous solids by the modified single-pellet moment technique. The Darcy coefficient, together with effective diffusion coefficients, was determined for an inert tracer.

In the present study, the moment theory was developed for nonisobaric conditions for an adsorbing gas, and used for the evaluation of effective diffusivities and contributions of viscous flow, surface diffusion, and Knudsen flow on the permeability of gases such as hydrogen, carbon dioxide, and helium in alumina and in Pd-impregnated alumina pellets.

Method and Theory

Nonisobaric pulse-response experiments were carried out with the dynamic version of the Wicke-Kallenbach type of a diffusion cell. The diffusion cell used in this work is shown in Figure 1. For the evaluation of transport parameters, a pulse of adsorptive or inert tracer was injected into the carrier gas flowing through the upper chamber of the diffusion cell, and the response peaks were obtained at the exit stream leaving the lower chamber, using a thermal conductivity detector. It was shown in the literature (Dogu and Smith, 1975; Dogu et al., 1989) that the mass-transfer resistance between gas and the pellet surface was negligible in this system. Pulse-response experiments were carried out at different pressure differences between the upper and lower faces of the pellet.

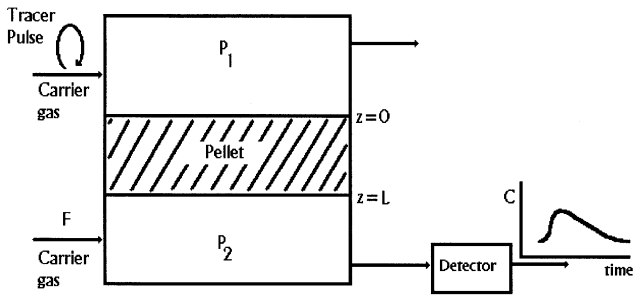

Figure 1. Diffusion cell.

Details of the method and justification of the assumptions were reported in previous publications (Dogu and Smith, 1975, 1976; Dogu et al., 1989; Kopac et al., 1996).

The experimental values of the zeroth and first moments were obtained from the response peaks using the following equation

$$m_n = \int_0^\infty C(t) t^n \, dt \qquad n = 0, 1, \ldots. \tag{1}$$

At nonisobaric conditions, the differential mass balance for transport of the diffusing component i (adsorbing gas) within the pellet is

$$(\epsilon + \rho_p K)\frac{\partial y_i}{\partial t} = D_e \frac{\partial^2 y_i}{\partial z^2} - \gamma \frac{\partial y_i}{\partial z} \tag{2}$$

for small variations of total concentration across the pellet. Here, the term γ contains the contributions of viscous flow, Knudsen flow, and surface diffusion flow

$$\gamma = \frac{(-\Delta P)}{L} \times \left[\underbrace{\frac{a^2\epsilon}{8\mu}\left(\frac{1}{\tau_v}\right)}_{\text{viscous flow}} + \underbrace{\frac{D_{KA}\epsilon}{P}\left(\frac{\phi}{\tau_k}\right)}_{\text{Knudsen flow}} + \underbrace{\frac{D_s \rho_p K}{P\tau_s}}_{\text{surface diffusion flow}} \right] \tag{3}$$

The viscous flow contribution can also be expressed as

$$\gamma_v = \frac{(-\Delta P)}{L}\frac{a^2\epsilon}{8\mu}\left(\frac{1}{\tau_v}\right) = \frac{(-\Delta P)}{L}\frac{C_o}{\mu} \tag{4}$$

where C_o is the Darcy coefficient. For porous solids with small pores, at low pressures Knudsen flow may become the predominant transport mechanism (Keizer et al., 1988). The parameter ϕ that appears in the Knudsen flow term was derived from the dusty gas model (Allawi and Gunn, 1987; Beuscher and Gooding, 1998) and may be expressed as

$$\phi = \frac{D_{AB} + D_{KB}}{(D_{AB} + D_{KA}) + (D_{KB} - D_{KA})y_A} \tag{5}$$

For a pure component, ϕ becomes unity. However, for a binary system with low concentration of A it may be approximated as

$$\phi = \frac{D_{AB} + D_{KB}}{(D_{AB} + D_{KA})}; \qquad \text{(dilute system)} \tag{6}$$

For strongly adsorbing gases, the contribution of surface diffusion to γ might also be significant, especially at low temperatures and at high pressures. The tortuosity factors τ_v, τ_k, and τ_s corresponding to the viscous flow, Knudsen flow, and surface diffusion terms are not necessarily equal to each other. In particular, τ_s was expected to be different than the viscous and Knudsen flow tortuosity factors. As a first approximation, the τ_v and τ_k terms may be taken to be equal.

As was shown in our previous work, the surface diffusion of hydrogen becomes significant in Pd-alumina pellets at low temperatures even for an isobaric system (Dogan and Dogu, 2003). The effective diffusion coefficient (in Eq. 2) may be expressed (Okubo and Inoue, 1988) as

$$D_e = \frac{\epsilon}{\tau}\left[\frac{1}{\frac{1}{D_{KA}} + \frac{1}{D_{AB}}}\right] + \frac{\rho_p K D_s}{\tau_s} \tag{7}$$

The adsorption of the tracer was assumed to be reversible and intrinsically rapid so that the gas and adsorbed concentrations were in equilibrium at any time. The initial and boundary conditions assumed for the system are similar to that of Dogu et al. (1989)

$$t = 0 \qquad y_i = 0 \qquad 0 \le z \le L \tag{8}$$

$$z = 0 \qquad y_i = f(t) \tag{9}$$

$$z = L \qquad A\left(-D_e \frac{\partial y_i}{\partial z} + \gamma y_i\right)_{z=L} = F(y_i)_{z=L} \tag{10}$$

Here, $f(t)$ is the tracer input function (pulse input), F is the lower stream flow rate, and A is cross-sectional area of the pellet. The zeroth and first absolute moment expressions were determined from the solution of Eq. 2 in the Laplace domain

$$m_o = \frac{(\bar{f}_o)e^{\delta}}{\text{Cosh}\,\delta + \left(\frac{FL}{AD_e} - \delta\right)\frac{\text{Sinh}\,\delta}{\delta}} \tag{11}$$

where

$$\delta = \frac{\gamma L}{2D_e} \tag{12}$$

$$\bar{f}_o = \lim_{s \to 0} \bar{f}; \qquad \text{(zeroth moment of input function)} \tag{13}$$

$$\mu_1 = \frac{m_1}{m_o} = \mu_{1e} - \mu_{1f} = \frac{(\epsilon + \rho_p K)L^2}{2D_e} \times \frac{\left[\frac{\text{Sinh}\,\delta}{\delta} + \left(\frac{FL}{AD_e} - \delta\right)\left(\frac{\delta\,\text{Cosh}\,\delta - \text{Sinh}\,\delta}{\delta^3}\right)\right]}{\left(\text{Cosh}\,\delta + \left(\frac{FL}{AD_e} - \delta\right)\frac{\text{Sinh}\,\delta}{\delta}\right)} \tag{14}$$

Here, the first absolute moment for the pellet (μ_1) is the difference in the first absolute moments of response (μ_{1e}) and injection-pulse functions (μ_{1f}). The limiting form of the first moment expression for large values of the flow rate (F) can be expressed as

$$\mu_1 = \frac{(\epsilon + \rho_p K)L^2}{2D_e}\left[\frac{\text{Cosh}\,\delta}{\delta\,\text{Sinh}\,\delta} - \frac{1}{\delta^2}\right] \tag{15}$$

For the isobaric conditions ($\delta \to 0$), Eqs. 11 and 14 reduce to the following forms, respectively

$$m_{oo} = \frac{\bar{f}_o}{1 + \frac{FL}{AD_{eo}}} \tag{16}$$

$$\mu_{1o} = \frac{(\epsilon + \rho_p K)L^2}{6D_{eo}} \frac{\left(3\frac{A}{L}D_{eo} + F\right)}{\left(\frac{A}{L}D_{eo} + F\right)} \tag{17}$$

where the second subscript o denotes the isobaric condition. Equation 17 is similar to the form reported in the early work of Dogu and Smith (1976).

Experimental Work

In this study, aluminum hydroxide was produced analytically by the reaction of aluminum nitrate with urea at 90°C for 20 h. Aluminum hydroxide was fired at 1200°C to obtain alumina powder in alpha-form. XRD diffraction patterns (PW-3040 Philips) confirmed alpha-alumina (Figure 2). Alumina powder was mixed with Pd solution prepared by dissolving palladium chloride in hydrochloric acid. The solution concentration was adjusted to obtain a product that consisted of 3.1 g Pd for 100 g powder. After drying, reduction was made at 650°C for 10 h in a hydrogen atmosphere. XRD diffraction patterns of Pd-impregnated alumina are also shown in Figure 2. The diffraction intensities were found to decrease with Pd impregnation. Pellets of 2.5 cm in diameter and 1 cm and 0.2 cm in length were prepared by pressing the powder into the mold. Pure alumina pellets were also prepared at the same dimensions and almost at the same porosity. Alumina powder prepared in this work showed better pelletizing properties than commercial alumina powder. The physical properties of the pellets are given in Table 1. As is seen in Table 1, the mean pore radius of the Pd-alumina pellet is much higher than that of the pure alumina pellet. SEM photographs (LEO 435 VP) verified this result (Figure 3).

This work is the continuation of our previous work (Dogan and Dogu, 2003) where isobaric diffusion results were reported. In the present study, dynamic experiments were car-

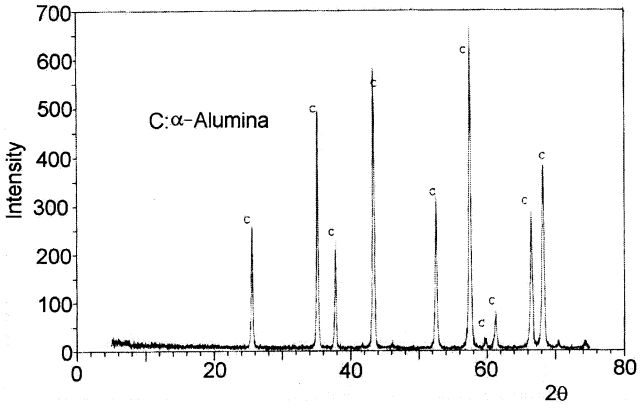

(a) Pure alumina

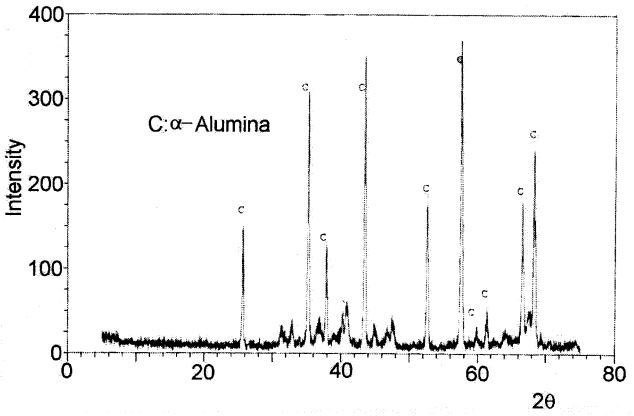

(b) 3.1 % Pd-alumina

Figure 2. XRD diffraction patterns of pure alumina and Pd-alumina powders.

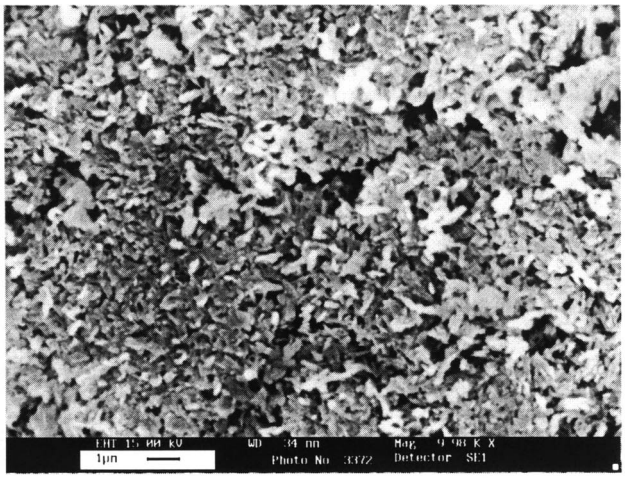

(a) Pure alumina pellet

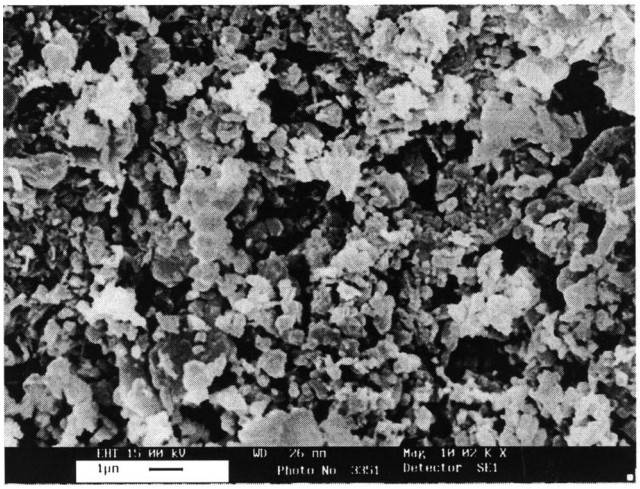

(b) 3.1% Pd-alumina pellet

Figure 3. SEM photographs of pure alumina pellet and 3.1% Pd-alumina pellet.

ried out at nonisobaric conditions. Nitrogen was used as the carrier gas with hydrogen and helium tracers, while helium was chosen as the carrier gas with a carbon dioxide tracer. The inlet volumetric flow rate of the upper stream was kept at 1.17 cm^3/s. The lower stream flow rate was changed from 1.2 cm^3/s to 6 cm^3/s, while pressure drop values across the pellet were kept at the adjusted values with a valve placed at the exit of the upper stream. The pressure of the tracer gas was adjusted to be the same as the pressure of the carrier gas in the upper chamber of the cell. Before entering the cell, the tracer gas was also preheated to the specified temperature of the experiment.

Nonisobaric experiments carried out with helium and carbon dioxide tracers were performed at 40°C, while experiments with hydrogen tracer were achieved at three different temperatures, namely, 40°C, 130°C, and 200°C. Nonisobaric experiments were carried out in a pressure-drop range of 2.8 kPa to 22.9 kPa across a pellet of 1 cm length. The reproducibility of the experimental results were justified by repeating most of the experiments at least twice.

The first absolute moment values of the response peaks contain contributions of the dead volumes. To obtain dead-

Table 1. Physical Properties of the Pellets Used in This Work (After Dogan and Dogu, 2003)

Physical Property	Pure Alumina Pellet	3.1% Pd-Alumina Pellet
Porosity (mercury porosimeter)	0.63	0.62
BET surface area, m^2/g (nitrogen adsorption)	44	24
Mean pore radius, nm (mercury porosimeter)	28	80
Tortuosity factor* (τ)	3.17	6.05

*Evaluated from isobaric inert tracer experiments at 40°C (Dogan and Dogu, 2003).

volume corrections, a set of pulse-response experiments were carried out with two pellets of the same porosity and with different lengths (1 cm and 0.2 cm). Differences in the first moments were used for the evaluation of effective diffusivities. The first absolute moment values for the pellet were then calculated using these diffusivity values in Eq. 17. From the differences between the experimental and calculated first moments, dead volume contributions were evaluated. All the experimental first absolute moment values were corrected for the dead-volume contributions. Corrected first absolute moment values reported in this article were then used in the evaluation of transport parameters.

Results and Discussion

Diffusion and flow parameters of helium tracer in alumina and Pd-alumina pellets

The dimensionless group δ, which is proportional to the ratio of viscous flow to diffusion fluxes, was evaluated from the zeroth moment data of helium tracer obtained at different pressure gradients. The ratio of zeroth moments obtained at isobaric and nonisobaric conditions can be expressed from Eqs. 11 and 16 as

$$\frac{m_{oo}}{m_o} = \frac{\text{Cosh}\,\delta + \left(\frac{FL}{AD_e} - \delta\right)\frac{\text{Sinh}\,\delta}{\delta}}{\left(1 + \frac{FL}{AD_{eo}}\right)e^{\delta}} \tag{18}$$

For large values of flow rate, F, this ratio reduces to (Dogu et al., 1989)

$$\frac{m_{oo}}{m_o} = \frac{D_{eo}\sinh\delta}{D_e\delta e^{\delta}} \tag{19}$$

The experimental values of the ratio m_{oo}/m_o obtained for the helium tracer at different pressure drops are shown in Figure 4. Figure 4 showed that m_{oo}/m_o values did not change appreciably by increasing lower stream flow rates. The dimensionless parameter δ was then evaluated using Eq. 19 and the data presented in Figure 4. Equations 18 and 19 also contain D_{eo} and D_e, which correspond to effective diffusivities in isobaric and nonisobaric conditions, respectively. The tortuosity factor of the pellets evaluated from isobaric diffusion experiments and the pore-size distributions were reported in our previous article (Dogan and Dogu, 2003). The physical properties of the pellets and the tortuosity factors (τ) are summarized in Table 1. Using the pore structure data,

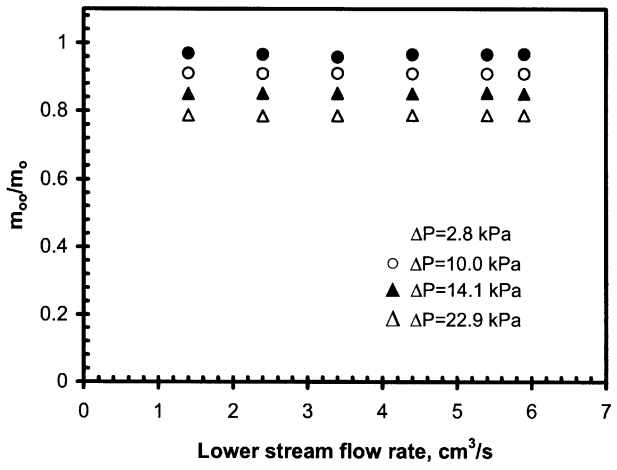

(a) Pure alumina pellet

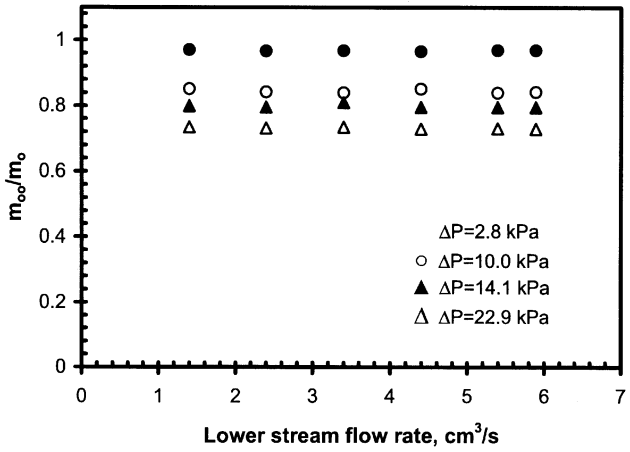

(b) Pd-alumina pellet

Figure 4. Variation of (m_{oo}/m_o) with respect to lower stream flow rate for helium tracer ($T = 40$°C, $L = 1$ cm).

the effective diffusivities were then evaluated at different pressures using Eq. 20

$$D_e = \frac{\epsilon}{\tau}\left[\frac{1}{\frac{1}{D_{KA}} + \frac{1}{D_{AB}}}\right] \tag{20}$$

Table 2. The Values of D_e, δ, and γ at Different Pressure-Drop Values for Helium Tracer ($T = 40$°C)

	Pure Alumina Pellet $\epsilon = 0.63$			3.1% Pd-Alumina Pellet $\epsilon = 0.62$		
ΔP, kPa	$D_e \times 10^6$, m²/s	δ	$\gamma \times 10^5$, m/s	$D_e \times 10^6$, m²/s	δ	$\gamma \times 10^5$, m/s
0	3.5	0	0	3.3*	0	0
2.8	3.5	0.03	2.3	3.3	0.033	3.4
10.0	3.5	0.087	8.0	3.2	0.222	12.0
14.1	3.4	0.19	11.3	3.2	0.270	16.9
22.9	3.4	0.28	18.4	3.1	0.400	27.4

*D_e values are from Dogan and Dogu (2003).

Table 3. Tortuosity (τ_v) Values Evaluated from Eq. 3 for Pure Alumina Pellet with Different Tracers

	Tortuosity				
ΔP, kPa	He in N_2 (40°C)	H_2 in N_2 (40°C)	H_2 in N_2 (130°C)	H_2 in N_2 (200°C)	CO_2 in He (40°C)
2.8	1.77	2.78	2.44	2.61	2.47
10.0	1.74	2.66	2.36	2.45	2.37
14.1	1.70	2.57	2.32	2.40	2.33
22.9	1.62	2.46	2.20	2.30	2.24

Table 4. Tortuosity (τ_v) Values Evaluated from Eq. 3 for Pd-Alumina Pellet with Different Tracers

	Tortuosity				
ΔP, kPa	He in N_2 (40°C)	H_2 in N_2 (40°C)	H_2 in N_2 (130°C)	H_2 in N_2 (200°C)	CO_2 in He (40°C)
2.8	2.98	3.58	3.77	4.07	6.94
10.0	2.86	3.35	3.58	3.86	6.69
14.1	2.79	3.20	3.50	3.78	6.66
22.9	2.67	3.08	3.46	3.60	6.46

The effective diffusivities evaluated by this procedure were then used in Eq. 19, and δ values were determined using the zeroth moment data. For both pure alumina and Pd-alumina pellets, the values of δ, γ, and D_e are tabulated in Table 2.

Helium is a nonadsorbing tracer and consequently no contribution of surface diffusion is expected. Assuming the same tortuosity for viscous and Knudsen flow terms ($\tau_v = \tau_k$), the flow tortuosities of alumina and Pd-alumina pellets were evaluated from Eq. 3 (using the γ values reported in Table 2), and the results were reported in Table 3. In these calculations, a dilute tracer assumption was made and ϕ values were evaluated from Eq. 6. For helium tracer (A) in nitrogen (B) Knudsen diffusivities and the average value of ϕ (average of values evaluated at different ΔP's) were $D_{KA} = 2.43 \times 10^{-5}$ m^2/s, $D_{KB} = 0.92 \times 10^{-5}$ m^2/s, and $\phi = 0.85$, respectively. Following a similar procedure, the tortuosity factor (τ_v) of the Pd-alumina pellet was also evaluated using the γ values evaluated at different pressure drops (Table 4). For this pellet, Knudsen diffusivities and the average value of ϕ value were $D_{KA} = 6.92 \times 10^{-5}$ m^2/s, $D_{KB} = 2.62 \times 10^{-5}$ m^2/s, and $\phi = 0.71$, respectively. The tortuosity factor of the Pd-alumina pellet, evaluated from the γ values, was found to be about 1.7 times larger than the tortuosity of the pure alumina pellet. A similar result was obtained for tortuosity factors (τ) evaluated from effective diffusivities obtained using isobaric pulse-response data (Table 1). It was interesting to note that tortuosity factor values (τ_v) evaluated from viscous and Knudsen flow, using Eq. 3 (Tables 3 and 4), were about half of the tortuosity factors (τ) evaluated from effective diffusivities obtained from isobaric pulse-response experiments (Table 1). In isobaric pulse-response experiments, diffusion into the dead-ended pores was also expected to contribute to the effective diffusivity, which would increase the tortuosity factor. However, such contributions were expected to be negligable in viscous flow.

Diffusion and flow parameters of hydrogen and carbon dioxide tracers in alumina and Pd-alumina pellets

Both hydrogen and carbon dioxide tracers were expected to adsorb on Pd-alumina and alumina pellets. Surface diffusion might also have some contribution to the diffusivity values of the adsorbing components. Effective diffusivities (D_{eo}) and adsorption equilibrium constants of both of these tracers obtained from isobaric pulse-response experiments in alumina and Pd-alumina pellets were reported in our previous work (Dogan and Dogu, 2003). The first moment expression (Eq. 14 or 15) contains the dimensionless parameter δ, effective diffusivity D_e, as well as the adsorption equilibrium constant $\rho_p K$. As was discussed in the previous section, the ratio of zeroth moments obtained under isobaric and nonisobaric conditions also contained the parameter δ and the effective diffusivities D_e and D_{eo} (Eq. 19). Knowing the D_{eo} and $\rho_p K$ values from the isobaric dynamic experiments, the other two unknowns, δ and the D_e, were then evaluated from the simultaneous analysis of the first absolute moment and zeroth moment data using Eqs. 19 and 14. The zeroth moment data and the corrected first absolute moment data obtained for the hydrogen tracer at 40°C in Pd-alumina and in pure alumina pellets are given in Figures 5 and 6, respectively. The unknown parameters D_e and δ were then determined from simultaneous analysis of these data and the results were summarized in Table 5.

The adsorption equilibrium constant of hydrogen on the Pd-alumina pellet was found to be about 50 times larger than the adsorption equilibrium constant obtained for pure alumina at 40°C (Table 5). This is due to the strong adsorption of hydrogen on palladium. At higher temperatures, the adsorption equilibrium constant becomes much smaller. Due to this high adsorption equilibrium constant of hydrogen obtained at 40°C, surface diffusion was also expected to make a contribution to the effective diffusivity for the Pd-alumina pellet. In fact, the effective diffusivities evaluated from Eq. 20, using the tortuosity factor (τ) found from the isobaric helium tracer data, were found to be smaller than the experimental values of effective diffusivities obtained for the hydrogen tracer in the Pd-alumina pellet, at 40°C. The surface diffusivity of hydrogen was then evaluated as $D_s/\tau_s = 3.0 \times 10^{-7}$ m^2/s, using Eq. 7 for the hydrogen tracer in Pd-alumina. For the pure alumina pellet and also for Pd-alumina pellet at higher temperatures (130°C and 200°C), the surface diffusion contribution was found to be negligible. For these cases, the experimental values of the effective diffusivities and the calculated values evaluated from Eq. 20 were quite close.

The tortuosity factor of alumina and Pd-alumina pellets corresponding to the viscous flow term (τ_v) were then evaluated from Eq. 3 using the data reported in Table 5. For hydrogen tracer in pure alumina, the Knudsen diffusivities, and the average values of ϕ were $D_{KA} = 3.43 \times 10^{-5}$ m^2/s, $D_{KB} = 0.92 \times 10^{-5}$ m^2/s, and $\phi = 0.78$, respectively, at 40°C. Viscous flow tortuosity factors evaluated from hydrogen tracer experiments, in alumina and Pd-alumina pellets, at different temperatures are reported in Tables 3 and 4, respectively.

A similar analysis was made for the carbon dioxide tracer (in helium) at 40°C. The zeroth and first absolute moment data obtained for the carbon dioxide tracer are given in Figures 7 and 8, respectively. The results of the simultaneous analysis of first and zeroth moment data are presented in Table 6. A comparison of experimental and calculated (from Eq. 20) effective diffusion coefficients were quite close, and it

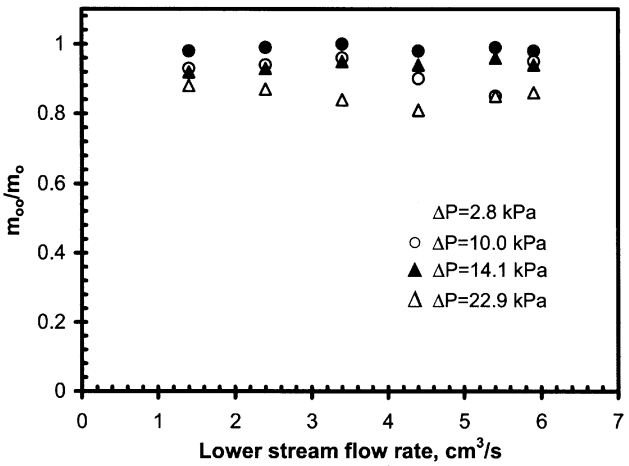

(a) Pure alumina pellet

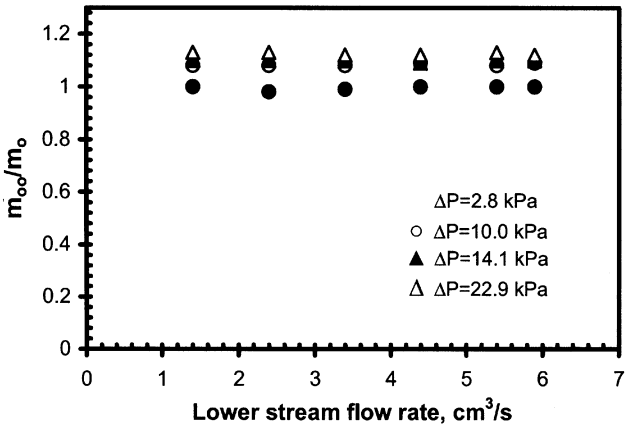

(b) Pd-alumina pellet

Figure 5. Variation of (m_{oo}/m_o) with respect to lower stream flow rate for hydrogen tracer ($T = 40$°C, $L = 1$ cm).

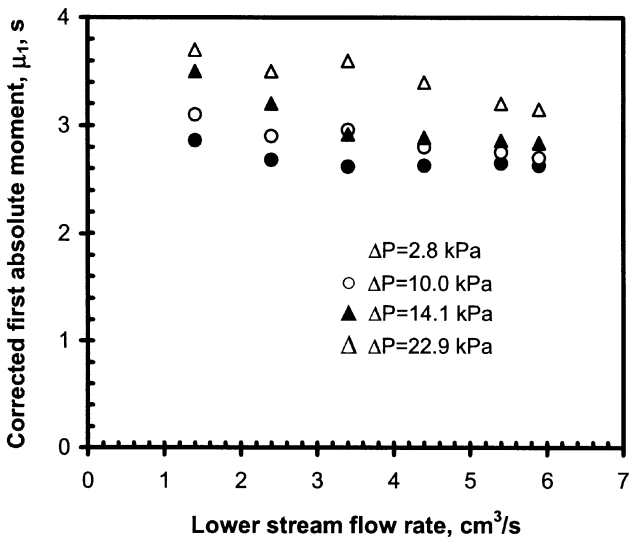

(a) Pure alumina pellet

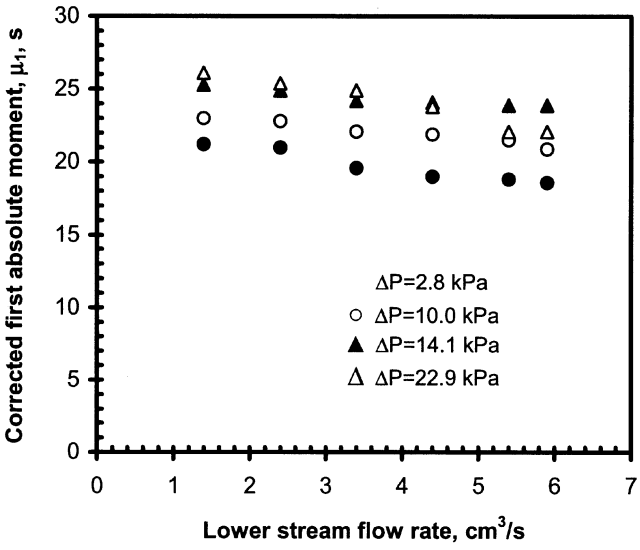

(b) Pd-alumina pellet

Figure 6. Variation of first absolute moments values with respect to lower stream flow rate for hydrogen tracer ($T = 40$°C, $L = 1$ cm).

was concluded that the surface-diffusion contribution was negligible for carbon dioxide in both alumina and Pd-alumina pellets. As is shown in Table 6, the adsorption equilibrium constant of carbon dioxide on pure alumina was higher than the adsorption equilibrium constant on Pd-alumina, which indicated that carbon dioxide was mostly adsorbed on alumina rather than on palladium.

Using the γ values of the carbon dioxide tracer (in helium) reported in Table 6, the flow tortuosity (τ_v) of the pellets was evaluated from Eq. 3; the results are summarized in Tables 3 and 4 for pure alumina and Pd-alumina pellets, respectively. For this case, Knudsen diffusivities of the carbon dioxide tracer, helium carrier, and the average value of ϕ were evaluated for the Pd-alumina pellet as 2.06×10^{-5} m^2/s, 6.92×10^{-5} m^2/s, and 1.57, respectively.

Permeabilities of hydrogen, carbon dioxide, and helium in alumina and Pd-alumina pellets

The flow tortuosity (τ_v) values evaluated using pulse-response data of different tracers were found to be quite close to each other. As is shown in Table 3, an average τ_v value of 2.29 could be used for the pure alumina pellet. Using this τ_v value, γ values were calculated for helium, hydrogen, and carbon dioxide tracers, and the results were compared with the experimental γ values in Figure 9. As is shown in this figure the correlation between the experimental and calculated γ values is quite good ($R^2 = 0.94$). These results showed that Eq. 3 is quite a good approximation of γ in nonisobaric diffusion experiments.

Following a similar procedure, γ values were also calculated for the Pd-alumina pellet. As is shown in Table 4, except for carbon dioxide, τ_v values evaluated from different tracers were also quite close for the Pd-alumina pellet. An

average τ_v value of 3.37 represents the tortuosities evaluated from dynamic experiments carried out with hydrogen and helium tracers. As is shown in Figure 10, experimental and calculated γ values (using $\tau_v = 3.37$ in Eq. 3) agreed well for these tracers. However, a higher τ_v value was obtained for carbon dioxide (Table 4). Consequently, the calculated γ values (using $\tau_v = 3.37$) caused an overestimation. This is also seen in Figure 10.

As was mentioned before, in the calculation of flow tortuosity (τ_v) from Eq. 3 using the experimental γ values, a dilute system assumption was made and ϕ values, which appeared in the Knudsen flow term of Eq. 3, were evaluated accordingly. In order to justify this assumption, the following criterion should hold (see Eq. 5)

$$\frac{(D_{KB} - D_{KA})y_A}{(D_{AB} + D_{KA})} \ll 1 \tag{21}$$

For helium and hydrogen tracers (in nitrogen), the value on the lefthand side of the inequality given in Eq. 21 is negative and less than $-0.25y_A$ for the alumina pellet. Considering that a 5 cm^3 pulse of tracer was injected into the nitrogen carrier gas, y_A was also expected to be quite less than unity, and neglecting the concentration-dependent term of the ϕ expression (Eq. 5) is acceptable. However, for the carbon dioxide tracer (in helium carrier gas), the lefthand side of the inequality given in Eq. 21 is positive and its value is about $0.55y_A$ for the Pd-alumina pellet. These results indicate that somewhat overestimated ϕ values could be obtained for the carbon dioxide tracer, especially in the Pd-alumina pellet. In fact, the ϕ value for this case was about 1.57, while for hydrogen and helium tracers (in nitrogen carrier gas), estimated ϕ values (assuming a dilute system) were around 0.8. With this dilute system assumption both the D_e and γ values become concentration independent and might cause some error in the estimation of τ_v from the experimental γ values. Higher τ_v values obtained with the carbon dioxide tracer in the Pd-alumina pellet might partly be due to this assumption. Our results also indicated that the most significant term of the γ expression (Eq. 3) was the Knudsen flow term.

The permeability of different tracers in porous solids/membranes are sometimes defined as

$$F_{o,i} = \frac{\gamma C}{\Delta P} \qquad \left(\text{mol/m}^2\ \text{s}\cdot\text{Pa}\right) \tag{22}$$

The average values of permeabilities evaluated at different pressure gradients across the pellet, for hydrogen, carbon dioxide, and helium tracers are reported in Table 7. The ratio of hydrogen to carbon dioxide permeabilities evaluated at 40°C for Pd-alumina and alumina pellet are

$$\left(\frac{F_{o,\text{H}_2}}{F_{o,\text{CO}_2}}\right)_{\text{alumina}} = 2.5; \qquad \left(\frac{F_{o,\text{H}_2}}{F_{o,\text{CO}_2}}\right)_{\text{Pd-alumina}} = 4.2$$

However, the ratio of helium to carbon dioxide permeabilities is about 3.0 for both alumina and the Pd-alumina pellet. This result indicated the positive effect of Pd impregnation in the alumina pellet to improve the separation of hydrogen from carbon dioxide. For the alumina pellet, the permeabilities obtained for hydrogen at different temperatures were about the same. However, for the Pd-alumina pellet, hydrogen permeability decreased with an increase in temperature. This result also indicated the contribution of surface diffusion to the permeability of hydrogen in Pd-alumina.

Conclusions

The nonisobaric pulse-response moment technique derived for adsorptive tracers was shown to give detailed information about the contributions of Knudsen flow, viscous flow, and surface flow terms on the permeability as well as effective diffusivity in porous solids, from a single set of experimental results. It was shown that tortuosity factors evaluated from the effective diffusivities obtained from isobaric pulse-response experiments were somewhat higher than the tortuosity factors evaluated from the viscous and Knudsen flow

Table 5. The Values of D_e, δ, and γ at Different Pressure-Drop Values for Hydrogen Tracer

		Pure Alumina Pellet				3.1% Pd-Alumina Pellet			
	ΔP, kPa	$D_e \times 10^6$, m^2/s	δ	$\gamma \times 10^5$, m/s	$\rho_p K^*$	$D_e \times 10^6$, m^2/s	δ	$\gamma \times 10^5$, m/s	$\rho_p K^*$
$T = 40$°C	0	5.0*	0	0	0.13	7.6*	0	0	6.97
	2.8	4.8	0.04	1.9		6.8	0.09	4.0	
	10.0	4.7	0.06	6.8		6.1	0.14	14.4	
	14.1	4.5	0.12	9.6		5.3	0.28	20.3	
	22.9	4.0	0.19	15.6		5.8	0.19	33.0	
$T = 130$°C	0	5.1*	0	0	0.09	6.3*	0	0	1.42
	2.8	5.0	0.02	2.6		5.8	0.09	3.9	
	10.0	4.0	0.18	9.1		5.5	0.13	13.9	
	14.1	4.0	0.14	12.8		5.2	0.20	19.6	
	22.9	4.0	0.22	20.8		4.8	0.29	31.9	
$T = 200$°C	0	5.3*	0	0	0.06	6.4*	0	0	0.60
	2.8	5.2	0.03	2.7		6.0	0.11	4.1	
	10.0	4.5	0.16	9.8		5.8	0.14	14.6	
	14.1	4.5	0.18	13.8		5.3	0.23	20.6	
	22.9	4.3	0.22	22.3		5.2	0.27	33.5	

(*) ρ_p, K and D_e values are from Dogan and Dogu (2003).

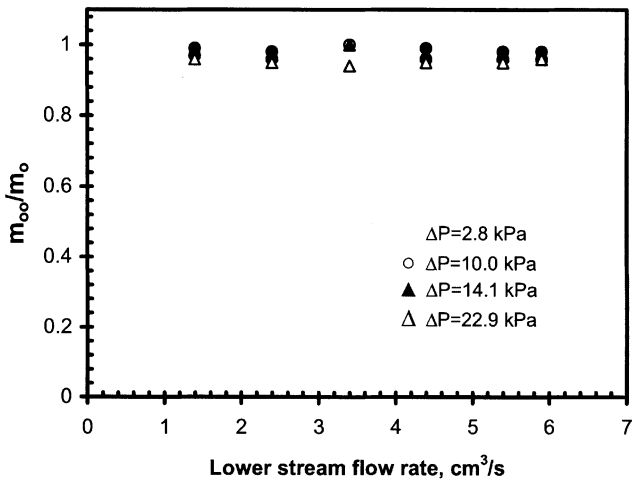

(a) Pure alumina pellet

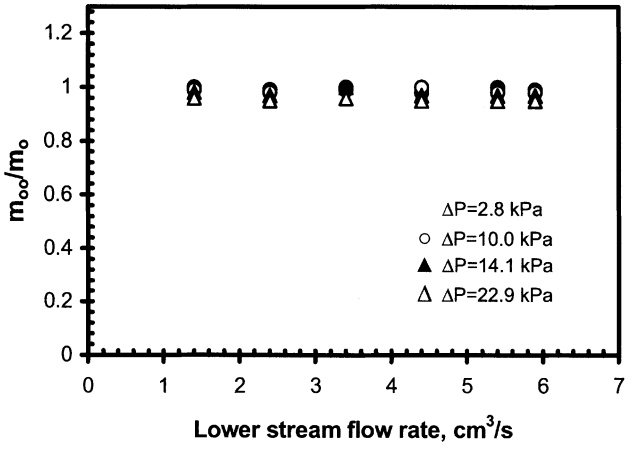

(b) Pd-alumina pellet

Figure 7. Variation of (m_{oo}/m_o) with respect to lower stream flow rate for carbon dioxide tracer ($T = 40°C$, $L = 0.2$ cm).

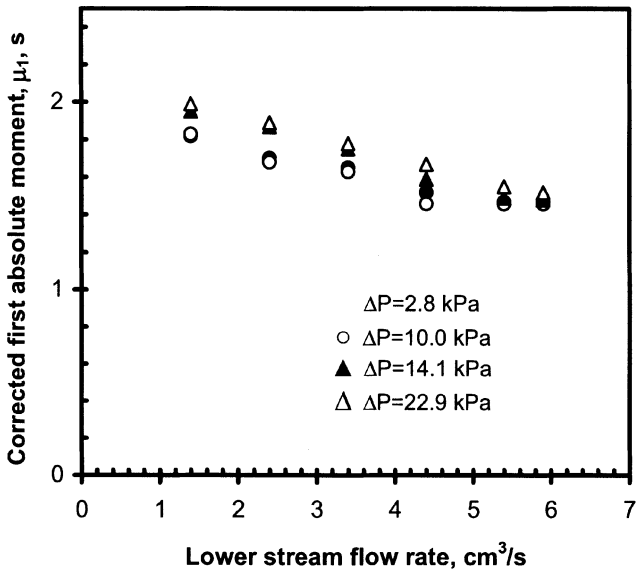

(a) Pure alumina pellet

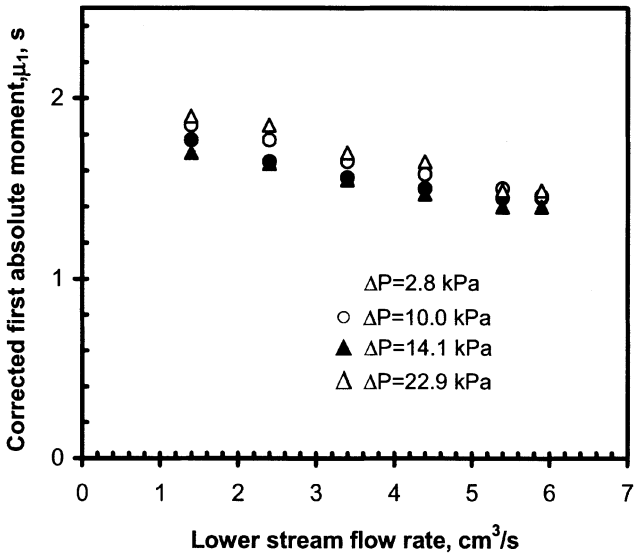

(b) Pd-alumina pellet

Figure 8. Variation of first absolute moments values with respect to lower stream flow rate for carbon dioxide tracer ($T = 40°C$, $L = 0.2$ cm).

terms. This was attributed to the contribution of dead-ended pores to the tortuosity, in the case of dynamic isobaric diffusion experiments. Some enhancement of hydrogen permeability was observed due to Pd impregnation in alumina pellets. It was concluded that the surface flow contribution to

Table 6. The Values of D_e, δ, and γ at Different Pressure Drops for Carbon Dioxide Tracer ($T = 40°C$)

	Pure Alumina Pellet $\epsilon = 0.63$				3.1% Pd-Alumina Pellet $\epsilon = 0.62$			
ΔP, kPa	$D_e \times 10^6$, m^2/s	δ	$\gamma \times 10^5$, m/s	$\rho_p K^*$	$De \times 10^6$, m^2/s	δ	$\gamma \times 10^5$, m/s	$\rho_p K^*$
0	1.2*	0	0		1.00*	0	0	
2.8	1.2	0.0096	0.72		0.98	0.0158	0.97	
10.0	1.2	0.0140	2.60	2.07	0.97	0.0500	3.50	1.50
14.1	1.2	0.0170	3.60		1.00	0.0200	4.90	
22.9	1.1	0.0655	5.90		0.94	0.1100	8.00	

(*) ρ_p, K, and D_e values are from Dogan and Dogu (2003).

Table 7. Permeabilities (from Eq. 22) of Different Tracers in Pure Alumina and Pd-Alumina Pellets

	$F_o \times 10^7$ (mol/m^2 s Pa)				
	He in N_2 (40°C)	H_2 in N_2 (40°C)	H_2 in N_2 (130°C)	H_2 in N_2 (200°C)	CO_2 in He (40°C)
Pure alumina pellet	3.0	2.5	2.6	2.4	1.0
Pd-alumina pellet	4.4	5.5	4.0	3.6	1.3

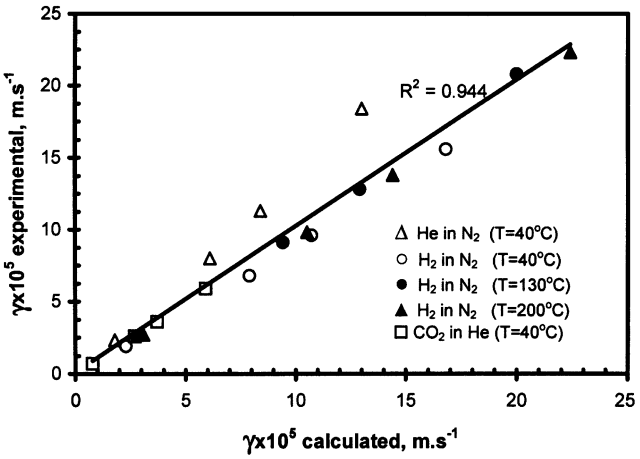

Figure 9. Experimental and calculated values of γ (from Eq. 3, using $\tau_v = \tau_k = 2.29$ for alumina pellet.

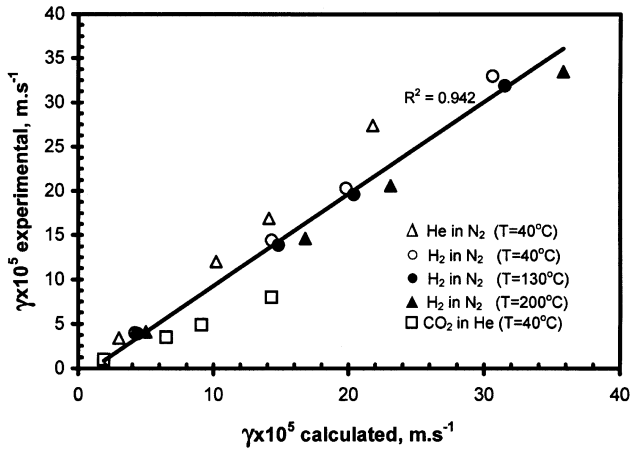

Figure 10. Experimental and calculated values of γ (from Eq. 3, using $\tau_v = \tau_k = 3.37$) for Pd-alumina pellet.

the permeation of hydrogen through Pd-impregnated alumina was significant at low temperatures.

Acknowledgment

Research Grant from TUBITAK (MISAG-143) and Gazi University Research Fund 06/2001-01 are appreciated. Discussions with Professor Timur Dogu of Middle East Technical University were more than helpful and highly appreciated.

Notation

a = mean pore radius, m
A = cross-sectional area of the pellet, m^2
C = total concentration, mole/m^3
C_o = Darcy coefficient, m^2
D_{AB} = molecular diffusivity of the molecule A in B, m^2/s
D_e = effective diffusivity in nonisobaric condition, m^2/s
D_{eo} = effective diffusivity in isobaric condition, m^2/s
D_{KA} = Knudsen diffusivity of A, m^2/s
D_{KB} = Knudsen diffusivity of B, m^2/s
D_s = surface diffusivity, m^2/s
$\bar{f}$ = Laplace transform of the function $f(t)$
$f(t)$ = tracer input function
$\bar{f}_o$ = defined in Eq. 13
F = lower stream flow rate, m^3/s
F_o = permeability, mol/m^2 s Pa
K = adsorption equilibrium constant, m^3/kg
L = length of the pellet, m
m_o = zeroth moment
m_1 = first moment
y_i = mole fraction of tracer
z = coordinate in the direction of diffusion in pellet, m

Greek letters

ΔP = pressure drop across the pellet, Pa
δ = defined by Eq. 12
ϵ = porosity of the pellet
ϕ = defined by Eq. 5
γ = defined by Eq. 3, m/s
μ = viscosity, Pa·s
μ_1 = first absolute moment for the pellet, s
μ_{1e} = first absolute moment of response, s
μ_{1f} = first absolute moment of injection-pulse functions, s
ρ_p = apparent density of the pellet, kg/m^3
τ = tortuosity factor evaluated from isobaric pulse-response experiments
τ_k = tortuosity factor corresponding to Knudsen flow
τ_s = tortuosity factor corresponding to surface diffusion flow
τ_v = tortuosity factor corresponding to viscous flow

Literature Cited

Allawi, Z. M., and D. J. Gunn, "Flow and Diffusion of Gases Through Porous Substrates," **33** (5), 766 (1987).
Beuscher, U., and C. H. Gooding, "The Permeation of Binary Gas Mixtures Through Support Structures of Composite Membranes," *J. Membr. Sci.*, **150**, 57 (1998).
Cerro, R. L., and J. M. Smith, "Chromatography of Nonadsorbable Gases," **16**, 1004 (1970).
Chai, M., Y. Yamashita, M. Machida, K. Eguchi, and H. Arai, "Gas Permeation Through Microporous Alumina Membranes Containing Highly Dispersed Metal Particles," *Chem. Lett.*, **6**, 979 (1992).
Champagnie, A. M., T. T. Tsotsis, R. G. Minet, and E. Wagner, "The Study of Ethane Dehydrogenation in a Catalytic Membrane Reactor," *J. Catal.*, **134**, 713 (1992).
Dogan, M., and G. Dogu, "Hydrogen Diffusivity Enhancement in Alumina Pellets Due to Impregnated Palladium," *Chem. Eng. Commun.*, **190** (5-8) 662 (2003).
Dogu, G., and J. M. Smith, "A Dynamic Method for Catalyst Diffusivities," *AIChE J.*, **21**, 58 (1975).
Dogu, G., and J. M. Smith, "Rate Parameters from Dynamic Experiments with Single Catalyst Pellets," *Chem. Eng. Sci.*, **31**, 123 (1976).
Dogu, G., A. Pekediz, and T. Dogu, "Dynamic Analysis of Viscous Flow and Diffusion in Porous Solids," *AIChE J.*, **35**, 1370 (1989).
Dougharty, N. A., "Effect of Adsorbent Particle-Size Distribution in Gas-Solid Chromatography," *AIChE J.*, **18**(3), 657 (1972).

Evans, R. B., G. M. Watson, and E. M. Mason, "Gaseous Diffusion in Porous Media. II. Effect of Pressure Gradients," *J. Chem. Phys.*, **36**(7), 1894 (1962).
Goto, S., S. Assabumrungrat, T. Tagawa, and P. Praserthdam, "The Effect of Direction of Hydrogen Permeation on the Rate Through a Composite Palladium Membrane," *J. Membr. Sci.*, **175**, 19 (2000).
Itoh, N., N. Tomura, T. Tsuji, and M. Hongo, "Deposition of Palladium Inside Straight Mesopores of Anodic Alumina Tube and its Hydrogen Permeability," *Microporous Mesoporous Mater.*, **39**, 103 (2000).
Keizer, K., R. J. R. Uhlhorn, R. J. Van Vuren, and A. J. Burggraaf, "Gas Separation Mechanisms in Microporous Modified γ-Al_2O_3 Membranes," *J. Membr. Sci.*, **39**, 285 (1988).
Konno, M., M. Shindo, S. Sugawara, and S. Saito, "A Composite Palladium and Porous Aluminum Oxide Membrane for Hydrogen Gas Separation," *J. Membr. Sci.*, **37**, 193 (1988).
Kopac, T., G. Dogu, and T. Dogu, "Single Pellet Reactor for the Dynamic Analysis of Gas-Solid Reactions—Reaction of SO_2 with Activated Soda," *Chem. Eng. Sci.*, **51**, 2201 (1996).
Kopac, T., "Non-Isobaric Adsorption Analysis of SO_2 on Molecular Sieve 13X and Activated Carbon by Dynamic Technique," *Chem. Eng. Process.*, **38**, 45 (1999).
Lee, S. J., S. M. Yang, and S. B. Park, "Synthesis of Palladium Impregnated Alumina Membrane for Hydrogen Separation," *J. Membr. Sci.*, **96**, 223 (1994).
Li, D., and S. Hwang, "Gas Separation by Silicon Based Inorganic Membrane at High Temperature," *J. Membr. Sci.*, **66**, 119 (1992).
Miller, J. R., and W. J. Koros, "The Formation of Chemically Modified γ-Alumina Microporous Membranes," *Sep. Sci. Technol.*, **25**, 1257 (1990).
Nicholson, D., and J. H. Petropoulos, "Capillary Models for Porous Media: V. Flow Properties of Random Networks with Various Radius Distributions," *J. Phys. D: Appl. Phys.*, **8**, 1430 (1975).
Nicholson, D., and J. H. Petropoulos, "Capillary Models for Porous Media: 8. Study of Gaseous Flow in Transition from Knudsen to Poiseuille Flow Regimes," *J. Phys. D: Appl. Phys.*, **11**(8), 1179 (1978).
Nicholson, D., and J. H. Petropoulos, "Correlation of Isothermal and Non-Isothermal Flow of Dilute Adsorbable Gases in Porous-Media," *J. Membr. Sci.*, **8**(2), 129 (1981).
Oktar, N., K. Murtezaoglu, G. Dogu, and T. Dogu, "Dynamic Analysis of Adsorption Equilibrium and Rate Parameters of Reactants and Products in MTBE, ETBE and TAME Production," *Can. J. Chem. Eng.*, **77**, 406 (1999).
Okubo, T., and H. Inoue, "Improvement of Surface Transport Property by Surface Modification," **34**, 1031 (1988).
Rodrigues, A. E., B. J. Ahn, and A. Zolalian, "Intraparticle Forced Convection Effect in Catalyst Diffusivity Measurements and Reactor Design," *AIChE J.*, **28**, 541 (1982).
Schneider, P., and J. M. Smith, "Adsorption Rate Constants from Chromatography," **14**, 767 (1968).
Scott, D. S., and A. L. Dullien, "Diffusion of Ideal Gases in Capillaries and Porous Solids," *AIChE J.,* **8**(1), 113 (1962).
So, J-H., S.-M. Yang, and S. B. Park, "Preparation of Silica-Alumina Composite Membranes for Hydrogen Separation by Multi-Step Pore Modifications," *J. Membr. Sci.*, **147**, 147 (1998).
Uemiya, S., M. Kajiwara, and T. Kojima, "Composite Membranes of Group VIII Metal Supported on Porous Alumina," **43**(11A), 2715 (1997).
Wakao, N., S. Otani, and J. M. Smith, "Significance of Pressure Gradients in Porous Materials: Part I. Diffusion and Flow in Fine Capillaries," *AIChE J.*, **11**(3), 435 (1965).

Manuscript received Nov. 11, 2002, and revision received May 9, 2003.